*Progress In Electromagnetics Research, PIER 43, 1–37, 2003*

# COMPARISON BETWEEN FREQUENCY DOMAIN AND TIME DOMAIN METHODS FOR PARAMETER RECONSTRUCTION ON NONUNIFORM DISPERSIVE TRANSMISSION LINES

**J. Lundstedt**

Ericsson Radio Systems AB
SE-164 80 Stockholm, Sweden

**M. Norgren**

Division of Electromagnetic Theory
Alfvén Laboratory
Kungliga Tekniska Högskolan
SE-100 44 Stockholm, Sweden

**Abstract**—In this paper, we present two methods for the inverse problem of reconstructing a parameter profile of a nonuniform and dispersive transmission line — one frequency domain and one time domain method. Both methods are based on the wave splitting technique, but apart from that the methods are mathematically very different. The time domain analysis leads to hyperbolic partial differential equations and an inverse method based on solving implicit equations. The frequency domain analysis leads instead to Riccati differential equations and an inverse method based on optimization. The two methods are compared numerically by simulating a reconstruction of a soil moisture profile along a flat band cable. A heuristic model of the dispersion characteristics of a flat band cable in moist sand is derived. We also simulate the effect parasitic capacitances at the cable ends has on the reconstructions. The comparison shows that neither method outperforms the other. The time domain method is numerically much faster whereas the frequency domain method is much faster to implement. An important conclusion is also that it is crucial to model the connector parasitic capacitances correctly — especially if there are impedance mismatches at the connectors.

## 1. INTRODUCTION

The inverse problem of parameter reconstruction on nonuniform transmission lines has been considered extensively over the past years. Primarily the reconstruction algorithms have been based on time domain (TD) methods [1, 2], but frequency domain (FD) methods have also been used [3, 4]. However, the developments of the algorithms in the two different domains have progressed in parallel with few — if any — comparisons in between by means of fourier transforms. One reason for this negligence may be that there has been the opinion that the reconstruction algorithm should be carried out in the frequency (time) domain if the scattering data are obtained from a frequency (time) domain measurement, since a numerically performed fourier transform between the two domains inevitably introduces additional errors in the measurement data. However, in a practical situation the choice of domain for the measurement is not determined by the reconstruction algorithm only. One must also take into account several practical considerations, like for example the sensitivity to calibration errors, whether the frequency spectrum is wide band or narrow band, the accessibility to a network analyzer (NWA) or a time domain reflectometer (TDR) etc.. Finally, an important criterion can be the dispersion characteristics of the transmission line, since certain dispersion model might be more suited for frequency domain algorithms while others might be better suited for time domain algorithms. These and other considerations determine whether the measurements shall be conducted in the frequency domain or in the time domain, and whether to use a frequency domain or time domain inverse algorithm.

In this paper we consider two methods for parameter reconstruction on nonuniform dispersive transmission lines — one frequency domain method and one time domain method. As a suitable case study, we have chosen the reconstruction of the water content in moist sand through measurements of the reflected voltage from a flat band cable buried in the sand. Our intentions are to compare the solutions to the direct problem using the frequency domain and time domain direct solvers, respectively, and to compare the reconstructions obtained when using the FD and TD inverse algorithms, respectively, on artificial noisy measurement data that has been generated either in the frequency domain or in the time domain. In a practical situation, geometrical differences at the connection points of the nonuniform transmission line give rise to stray capacitances. The influences of such stray capacitances on the performances of the reconstruction algorithms are also investigated.

The disposition of the article is as follows: The scattering problem and model equations are described in Section 2. In Section 3, approximate dispersion models for the parameters are derived and the values of the electrical parameters are given. In Sections 4 and 5, we derive the solutions to the direct scattering problem on a nonuniform dispersive transmission in the frequency domain and in the time domain, respectively. In Sections 6 and 7, we derive the reconstruction algorithms for the inverse scattering problem on a nonuniform dispersive transmission in the frequency domain and in the time domain, respectively. Numerical results are presented in Section 8, and Section 9 contains the conclusions.

## 2. PROBLEM FORMULATION

Consider a nonuniform transmission line (NTL) of length $l$, situated between $x = 0$ and $x = l$. The nonuniform line is connected, via uniform transmission lines at both ends, to a network analyzer (NWA) or time domain reflectometer (TDR); see Figure 1. The transmission lines to the left and right have the characteristic impedances $Z_0$ and $Z_l$, respectively.

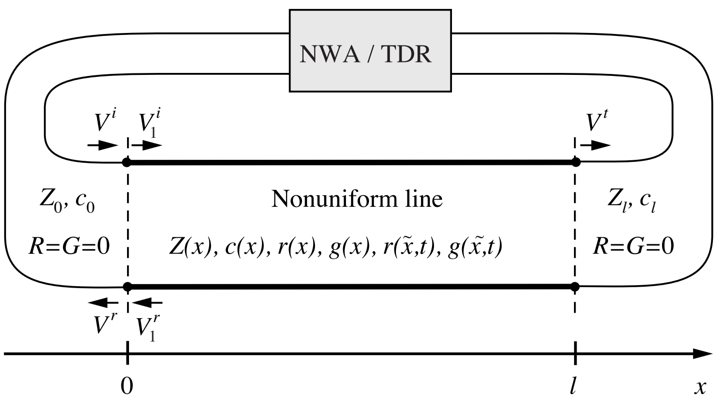


**Figure 1.** A dispersive nonuniform transmission line of length $l$, is connected to a NWA (or TDR) via nondispersive uniform transmission lines at both ends.

Assuming that the wave propagation is dominated by the quasi-TEM mode, we can model the transient signal propagation along the nonuniform and dispersive transmission line with the transmission line equations,

$$\partial_x \hat{V}(x,\omega) = -\left(\hat{\boldsymbol{R}}(x,\omega) + \mathrm{j}\omega\hat{\boldsymbol{L}}(x,\omega)\right)\hat{I}(x,\omega), \qquad (1)$$

$$\partial_x \hat{I}(x,\omega) = -\left(\hat{\boldsymbol{G}}(x,\omega) + \mathrm{j}\omega\hat{\boldsymbol{C}}(x,\omega)\right)\hat{V}(x,\omega), \tag{2}$$

which in the time domain become

$$\partial_x V(x,t) = -\left(\boldsymbol{R}(x,t) * + \boldsymbol{L}(x,t) * \partial_t\right) I(x,t), \tag{3}$$
$$\partial_x I(x,t) = -\left(\boldsymbol{G}(x,t) * + \boldsymbol{C}(x,t) * \partial_t\right) V(x,t). \tag{4}$$

$V(x,t)$ and $I(x,t)$ denote the voltage and current at position $x$, respectively. $\partial_x$ and $\partial_t$ denote differentiation with respect to $x$ and $t$, respectively. The symbol $*$ denotes a convolution integral with respect to time, and should be understood as follows:

$$f_1(t) * f_2(t) = \int_0^t f_1(t - t') f_2(t') \, \mathrm{d}t'. \tag{5}$$

$\boldsymbol{L}, \boldsymbol{C}, \boldsymbol{R}$ and $\boldsymbol{G}$ denote the distributed inductance, capacitance, series resistance and shunt conductance of the transmission line, respectively. The hat symbol denotes the Fourier transform of a function, e.g., $\hat{\boldsymbol{L}}(x,\omega)$ is the Fourier transform of $\boldsymbol{L}(x,t)$. Note that $\boldsymbol{L}(x,t), \boldsymbol{C}(x,t), \boldsymbol{R}(x,t)$ and $\boldsymbol{G}(x,t)$ are dispersion kernels in the time domain transmission line equations

## 3. DISPERSION MODEL AND FORMULATION OF THE INVERSE PROBLEM

An example of a strongly dispersive transmission line is a flat band cable surrounded by moist sand. Since water is highly dispersive, the effect of the moist sand on the electrical parameters will make the transmission line dispersive. If a model relating the electrical parameters and the soil moisture can be determined, the soil moisture can be determined from electrical measurements on the transmission line.

To keep the analysis simple and illustrative, we develop a heuristical dispersion model in the frequency domain. This model is then transformed to the time domain.

### 3.1. The Dispersion Model in the Frequency Domain

The flat band cable consists of three strip conductors embedded in a plastic band; see Figure 2. We assume that the even mode is excited, i.e., the two outer conductors have the same potentials.

We consider the surrounding medium as a mixture of sand, water and air. Since there are no pronounced magnetic properties in the surrounding medium, we make the approximations that the series

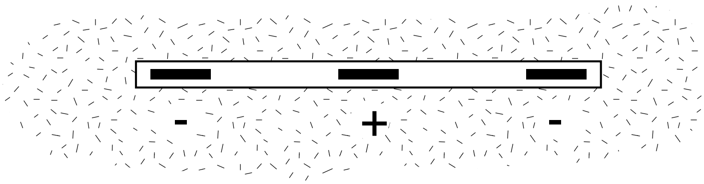


**Figure 2.** Cross section of the flat band cable in sand.

inductance $\hat{\boldsymbol{L}}$ is not affected by the surrounding moist soil, and that the inductance is nondispersive, i.e.,

$$\hat{\boldsymbol{L}}(x,\omega) = L_{\rm b}, \tag{6}$$

where $L_{\rm b}$ is the inductance of the flat band cable in free space. $\hat{\boldsymbol{L}}(x,\omega)$ is thus independent of the position $x$ and considered as non dispersive, in the frequency interval of interest.

In the direction of the band cable, the surrounding medium is described by a relative permittivity $\hat{\varepsilon}_{\rm r}(x,\omega)$ that depends on the position $x$ and the angular frequency $\omega$. The effective permittivity of this three phase mixture can be determined by means of effective medium theories; see e.g., [5]. However, in order to avoid a too complicated material model in the inverse problem, we estimate the effective relative permittivity from the upper Wiener bound, which is the extremum obtained when all phases are arranged in parallel with the direction of the applied field. The upper Wiener bound for our mixture is

$$\hat{\varepsilon}_{\rm r}(x,\omega) = (1-\nu)\,\varepsilon_{\rm rock} + 1\cdot\nu\,(1-q(x)) + \nu q(x)\,\hat{\varepsilon}_{\rm water}(\omega), \tag{7}$$

where $\nu$ is the relative pore-volume, $\varepsilon_{\rm rock}$ is the relative permittivity for solid rock (the sand grains), $\hat{\varepsilon}_{\rm water}(\omega)$ is the frequency dependent and complex valued relative permittivity for water, and where $q(x)$ is the relative water content in the pore-volumes. $q(x)$ is defined as the *moisture parameter*. Thus, the inverse problem is to determine $q$ as a function of the position $x$ along the band cable. Using the relation

$$\hat{\varepsilon}_{\rm water}(\omega) = 1 + \hat{\chi}_{\rm water}(\omega), \tag{8}$$

where $\hat{\chi}_{\rm water}(\omega)$ is the electric susceptibility of water, (7) can be written as

$$\hat{\varepsilon}_{\rm r}(x,\omega) = \varepsilon_{\rm sand} + \nu q(x)\,\hat{\chi}_{\rm water}(\omega), \tag{9}$$

where

$$\varepsilon_{\rm sand} = (1-\nu)\,\varepsilon_{\rm rock} + \nu, \tag{10}$$

is the upper bound for the relative permittivity of dry sand. If possible, $\varepsilon_{\mathrm{sand}}$ should be determined from a measurement on dry sand, instead of using (10).

At frequencies below 60 GHz, the electric susceptibility of water can be described with the Debye model [6]

$$\hat{\chi}_{\mathrm{water}}(\omega) = \varepsilon_\infty + \frac{\varepsilon_{\mathrm{s}} - \varepsilon_\infty}{1 + \mathrm{j}\omega\tau_{\mathrm{d}}} - 1, \tag{11}$$

in which $\varepsilon_{\mathrm{s}}$ is the relative permittivity for static fields, $\tau_{\mathrm{d}}$ is the Debye relaxation time, and $\varepsilon_\infty$ is the optical response [5]; the contribution from the fast processes in the medium to the permittivity at moderate frequencies.

The total shunt capacitance between the inner conductor and the two outer conductors (even mode) in an insulated band cable embedded in moist sand (see Figure 2) is estimated with the following formula:

$$\hat{C}(x,\omega) = C_1 + \frac{C_2 \cdot \hat{\varepsilon}_{\mathrm{r}}(x,\omega)\, C_3}{C_2 + \hat{\varepsilon}_{\mathrm{r}}(x,\omega)\, C_3}. \tag{12}$$

In (12), $C_1, C_2$ and $C_3$ can be interpreted as geometrical part capacitances for a band cable surrounded with vacuum; $C_1$ is the capacitance inside the insulator between the conductors; $C_2$ emanates from the capacitances between the conductors and the surfaces of the insulator; $C_3$ is the exterior capacitance between the $C_2$ parts; see Figure 3. The presence of $\hat{\varepsilon}_{\mathrm{r}}(x,\omega)$ in (12) implies a surrounding medium that differs from vacuum.

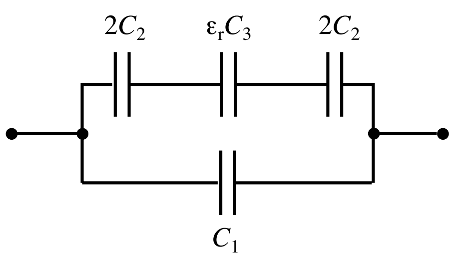


**Figure 3.** Circuit model for the total shunt capacitance.

Using (11) and (9) in (12), it follows that the total capacitance is described by the Debye model

$$\hat{C}(x,\omega) = C_\infty(x) + \frac{C_{\mathrm{s}}(x) - C_\infty(x)}{1 + \mathrm{j}\omega\tau_{\mathrm{eff}}(x)}, \tag{13}$$

where

$$C_\infty(x) = C_1 + \frac{C_2 C_3 (\varepsilon_{\text{sand}} + \nu q(x)(\varepsilon_\infty - 1))}{C_2 + C_3 (\varepsilon_{\text{sand}} + \nu q(x)(\varepsilon_\infty - 1))}, \tag{14}$$

$$C_{\text{s}}(x) = C_1 + \frac{C_2 C_3 (\varepsilon_{\text{sand}} + \nu q(x)(\varepsilon_{\text{s}} - 1))}{C_2 + C_3 (\varepsilon_{\text{sand}} + \nu q(x)(\varepsilon_{\text{s}} - 1))}, \tag{15}$$

$$\tau_{\text{eff}}(x) = \tau_{\text{d}} \frac{C_2 + C_3 (\varepsilon_{\text{sand}} + \nu q(x)(\varepsilon_\infty - 1))}{C_2 + C_3 (\varepsilon_{\text{sand}} + \nu q(x)(\varepsilon_{\text{s}} - 1))}. \tag{16}$$

$C_\infty$ is the optical response of the capacitance, $C_{\text{s}}$ is the static capacitance, and $\tau_{\text{eff}}$ is the effective relaxation time. Note that all parameters in (13) depend on the local value of the moisture parameter $q(x)$.

If we allow the parameters in equations (1) and (2) to be complex valued, there will be a seeming ambiguity in the separation into dissipative and reactive parameters. For example, if all electrical losses are attributed to the imaginary part of the complex valued capacitance $\hat{C}(x)$, we have in the view of equation (2) that

$$\hat{\boldsymbol{C}}(x,\omega) = \hat{C}(x,\omega), \qquad \hat{\boldsymbol{G}}(x,\omega) = 0. \tag{17}$$

On the other hand, if we require both $\hat{\boldsymbol{C}}$ and $\hat{\boldsymbol{G}}$ to be real valued we obtain

$$\hat{\boldsymbol{C}}(x,\omega) = \operatorname{Re}\left\{\hat{C}(x,\omega)\right\}, \qquad \hat{\boldsymbol{G}}(x,\omega) = -\omega \operatorname{Im}\left\{\hat{C}(x,\omega)\right\}. \tag{18}$$

In the present paper we will use (17), since it yields a shorter notation in the FD analysis and is more appropriate in a problem involving dielectric losses only; (18) is appropriate when the losses are dominated by a static conductivity. The series resistance $\hat{\boldsymbol{R}}$ is considered to be negligible, i.e.,

$$\hat{\boldsymbol{R}}(x,\omega) = 0. \tag{19}$$

Hence, our frequency domain model for the electrical parameters of the flat band transmission line is given by equations (6), (9), (11), (13)–(16), (17) and (19), which involve the parameters $L_{\text{b}}$, $\varepsilon_{\text{sand}}$, $\nu$, $q$, $\varepsilon_\infty$, $\varepsilon_{\text{s}}$, $\tau_{\text{d}}$, $C_1, C_2$ and $C_3$.

## 3.2. The Dispersion Model in the Time Domain

The time domain model is obtained by taking the inverse fourier transforms of the parameters in the frequency domain model. We obtain

$$\boldsymbol{C}\left(x,t\right)=C_{\infty}\left(x\right)\delta\left(t\right)+\frac{C_{\mathrm{s}}\left(x\right)-C_{\infty}\left(x\right)}{\tau_{\mathrm{eff}}\left(x\right)}\mathrm{H}\left(t\right)\exp\left(\frac{-t}{\tau_{\mathrm{eff}}\left(x\right)}\right), \tag{20}$$

$$\boldsymbol{L}\left(x,t\right)=L_{\mathrm{b}}\delta\left(t\right), \tag{21}$$

$$\boldsymbol{R}\left(x,t\right)=\boldsymbol{G}\left(x,t\right)=0, \tag{22}$$

where $\delta\left(t\right)$ is Dirac's delta function and $\mathrm{H}\left(t\right)$ is Heaviside's step function. With $\boldsymbol{G}\left(x,t\right)=0$ it follows that all electric losses are included in the dispersion kernel $\boldsymbol{C}\left(x,t\right)$ for the capacitance. In conformance with the ambiguity in the frequency domain, one can transform from $\boldsymbol{C}\left(x,t\right)$ to another capacitance kernel and a nonzero conductance kernel; see also the discussion in Section 5.

### 3.3. The Values of the Electrical Parameters

The length of the band cable is chosen to $l=1\,\mathrm{m}$ and the characteristic impedances of the homogeneous transmission lines at $x=0$ and $x=l$, respectively, are chosen to $Z_0=Z_l=50\ \Omega$; see Figure 1.

In the comparison, the values of the electrical parameters are based on measurements on a flat band cable used for soil moisture determinations at the Institute for Meteorology and Climate research (IMK) in Karlsruhe, Germany. The parameters are the following:

$$C_1=3.5\ \mathrm{pF/m}, \tag{23}$$

$$C_2=340\ \mathrm{pF/m}, \tag{24}$$

$$C_3=16\ \mathrm{pF/m}, \tag{25}$$

$$L_{\mathrm{b}}=770\ \mathrm{nH/m}. \tag{26}$$

For the sand, the relative permittivity and pore volume are taken to be $\varepsilon_{\mathrm{sand}}=2.5$ and $\nu=0.45$, respectively.

At a temperature of 20° C, we have for water $\varepsilon_{\mathrm{s}}=80$, $\varepsilon_{\infty}=5,27$ and $\tau_{\mathrm{d}}=10\,\mathrm{ps}$. However, the relaxation time $\tau_{\mathrm{d}}=10\,\mathrm{ps}$ is very short in comparison with the round trip time, which is around 20 ns with our choice of electrical parameters. The rise time needed in the incident pulse for reconstructing a reasonable variation in the moisture parameter $q$ is therefore much longer than the relaxation time. Equivalently, the frequencies needed to resolve the variation in $q$ are much lower than the relaxation frequency in the Debye model. Thus, the medium reacts almost instantaneously and there will be no significant effects of the dispersion. Since we expect a much stronger influence from the dispersion if the relaxation time is comparable with the round trip time, we test the algorithms with different values of the Debye relaxation time $\tau_{\mathrm{d}}$: 10 ps, 1 ns, 10 ns and 1 $\mu$s.

# 4. THE DIRECT PROBLEM IN THE FREQUENCY DOMAIN

In this section, we solve the direct reflection problem in the frequency domain. Since the analysis is carried out at a fixed angular frequency $\omega$, the frequency dependencies of the voltage, current and the parameters are not written out explicitly. Following the analysis presented in [3], we collect the transmission line equations (1) and (2) into one ordinary differential equation (ODE) in a matrix form:

$$\begin{aligned}\partial_x \begin{pmatrix} \hat{V}(x) \\ \hat{I}(x) \end{pmatrix} &= \begin{pmatrix} 0 & -\hat{\boldsymbol{R}}(x) - \mathrm{j}\omega\hat{\boldsymbol{L}}(x) \\ -\hat{\boldsymbol{G}}(x) - \mathrm{j}\omega\hat{\boldsymbol{C}}(x) & 0 \end{pmatrix} \begin{pmatrix} \hat{V}(x) \\ \hat{I}(x) \end{pmatrix} \\ &= \hat{D}(x) \begin{pmatrix} \hat{V}(x) \\ \hat{I}(x) \end{pmatrix}. \end{aligned} \tag{27}$$

## 4.1. Wave Splitting and the Riccati Equation

We transform the dependent variables from the voltage $\hat{V}$ and the current $\hat{I}$ to the split voltages, denoted $\hat{V}^+$ and $\hat{V}^-$, through the following wave-splitting:

$$\begin{pmatrix} \hat{V}^+(x) \\ \hat{V}^-(x) \end{pmatrix} \frac{1}{2} \begin{pmatrix} 1 & Z_0 \\ 1 & -Z_0 \end{pmatrix} \begin{pmatrix} \hat{V}(x) \\ \hat{I}(x) \end{pmatrix} S_0 \begin{pmatrix} \hat{V}(x) \\ \hat{I}(x) \end{pmatrix}, \tag{28}$$

for which the inverse transformation from split voltages to voltage and current reads

$$\begin{pmatrix} \hat{V}(x) \\ \hat{I}(x) \end{pmatrix} \begin{pmatrix} 1 & 1 \\ Y_0 & -Y_0 \end{pmatrix} \begin{pmatrix} \hat{V}^+(x) \\ \hat{V}^-(x) \end{pmatrix} S_0^{-1} \begin{pmatrix} \hat{V}^+(x) \\ \hat{V}^-(x) \end{pmatrix}, \tag{29}$$

where $Y_0 = Z_0^{-1}$. Using (28) and (29) in (27), we obtain the ODE for the split voltages:

$$\partial_x \begin{pmatrix} \hat{V}^+(x) \\ \hat{V}^-(x) \end{pmatrix} S_0 \hat{D}(x) S_0^{-1} \begin{pmatrix} \hat{V}^+(x) \\ \hat{V}^-(x) \end{pmatrix} = \begin{pmatrix} -\hat{a}(x) & -\hat{b}(x) \\ \hat{b}(x) & \hat{a}(x) \end{pmatrix} \begin{pmatrix} \hat{V}^+(x) \\ \hat{V}^-(x) \end{pmatrix}, \tag{30}$$

where

$$\hat{a}(x) = \frac{1}{2} \left( \mathrm{j}\omega \left( \hat{\boldsymbol{C}}(x) Z_0 + \hat{\boldsymbol{L}}(x) Y_0 \right) + \left( \hat{\boldsymbol{G}}(x) Z_0 + \hat{\boldsymbol{R}}(x) Y_0 \right) \right), \tag{31}$$

$$\hat{b}(x) = \frac{1}{2} \left( \mathrm{j}\omega \left( \hat{\boldsymbol{C}}(x) Z_0 - \hat{\boldsymbol{L}}(x) Y_0 \right) + \left( \hat{\boldsymbol{G}}(x) Z_0 - \hat{\boldsymbol{R}}(x) Y_0 \right) \right). \tag{32}$$

Using the wave-splitting (28), it follows that $\hat{V}^+$ and $\hat{V}^-$ are the incident and reflected voltages, respectively, on the uniform line in the region $x < 0$, and that the continuity of the voltage and the current is preserved for the split voltages. Thus, if we define the reflection coefficient $\hat{r}(x)$ from the relation

$$\hat{V}^-(x) = \hat{r}(x)\,\hat{V}^+(x)\,, \tag{33}$$

$\hat{r}(x)$ becomes the physical reflection coefficient for a subline (embedding geometry) $[x, l]$, of the original line $[0, l]$, connected to a uniform line with characteristic impedance $Z_0$. Using (30) and (33), we obtain the following Riccati equation for the reflection coefficient:

$$\partial_x \hat{r}(x) = 2\hat{a}(x)\,\hat{r}(x) + \hat{b}(x)\left(1 + \hat{r}^2(x)\right). \tag{34}$$

If the nonuniform part (with an impedance that differs from $Z_0$) recedes to $x = l$, we obtain the boundary condition

$$\hat{r}(l) = \frac{Z_l - Z_0}{Z_l + Z_0}, \tag{35}$$

for the reflection coefficient. Starting from (35) and integrating (34) in the $-x$ direction, we obtain the reflection coefficient $\hat{r}(x)$, for every subline $[x, l]$, and especially $\hat{\boldsymbol{r}} = \hat{r}(0)$, which is the reflection coefficient for the entire nonuniform transmission line.

### 4.2. Stray Capacitances at the Connections

If there are geometrical differences between the nonuniform line and the connected uniform lines, we can expect an increased capacitance in the vicinities of the connection points. Those stray capacitances are modeled with two lumped capacitors denoted $C_0$ and $C_l$, respectively. With the capacitor $C_l$ at $x = l$, the boundary condition (35) must be modified to

$$\hat{r}(l) = \frac{Z_l - Z_0\,(1 + \mathrm{j}\omega C_l Z_l)}{Z_l + Z_0\,(1 + \mathrm{j}\omega C_l Z_l)}. \tag{36}$$

With the capacitor $C_0$ at $x = 0$, the reflection coefficient (as seen from the supplying line) becomes

$$\hat{\boldsymbol{r}} = \frac{\hat{r}(0) - \mathrm{j}\omega C_0 Z_0\,(1 + \hat{r}(0))\,/2}{1 + \mathrm{j}\omega C_0 Z_0\,(1 + \hat{r}(0))\,/2}, \tag{37}$$

where $\hat{r}(0)$ has been determined from integration of (34), starting from (36).

## 5. THE DIRECT PROBLEM IN THE TIME DOMAIN

In this section we derive the mathematical equations needed to compute the reflected impulse response in the time domain.

In this work we allow the electrical parameters of the nonuniform transmission line to depend on both position and frequency. However, since all signals in practice have finite frequency contents, i.e. finite rise-times, we can separate the dispersion kernels into slowly and quickly varying parts. The quickly varying parts vary significantly faster than the signal varies. Hence, we can replace these parts by direct response terms. For example, let $\boldsymbol{L}(x,t) = \boldsymbol{L}_{\mathrm{f}}(x,t) + \tilde{L}(x,t)$, where $\boldsymbol{L}_{\mathrm{f}}(x,t)$ is the quickly varying part. The last term of equation (3) then becomes

$$\begin{aligned} \boldsymbol{L}(x,t) * \partial_t I(x,t) &= \Big(\boldsymbol{L}_{\mathrm{f}}(x,t) * \partial_t + \tilde{L}(x,t) * \partial_t\Big) I(x,t) \\ &\approx \Big(L(x)\,\partial_t + \tilde{L}(x,t) * \partial_t\Big) I(x,t), \end{aligned} \tag{38}$$

where

$$L(x) = \int_0^\infty \boldsymbol{L}_{\mathrm{f}}(x,t)\,\mathrm{d}t. \tag{39}$$

Integration by parts finally yields

$$\Big(L(x)\,\partial_t + \tilde{L}(x,t) * \partial_t\Big) I(x,t) \ \Big(L(x)\,\partial_t + \tilde{L}(x,0) + \tilde{L}_t(x,t) *\Big) I(x,t), \tag{40}$$

where the subscript $t$ denotes the time derivative of the dispersion kernel and the tilde symbol distinguishes the dispersion kernels from direct response parameters. $L(x)$ can be interpreted as the value of the inductance $\hat{\boldsymbol{L}}(x,\omega_{\mathrm{u}})$, where $\omega_{\mathrm{u}}$ is the upper limit of the frequency bandwidth of the signal.

In this way, we now rewrite equations (3) and (4) to obtain

$$\partial_x V(x,t) = -\Big(L(x)\,\partial_t + R(x) + \tilde{L}(x,0) + \tilde{R}(x,t) * + \tilde{L}_t(x,t) *\Big) I(x,t), \tag{41}$$

$$\partial_x I(x,t) = -\Big(C(x)\,\partial_t + G(x) + \tilde{C}(x,0) + \tilde{G}(x,t) * + \tilde{C}_t(x,t) *\Big) V(x,t). \tag{42}$$

From (41) and (42) we notice that $R(x)$, the direct response of the series resistance, and $\tilde{L}(x,0)$, the initial value of the inductance dispersion kernel, are equivalent from a signal propagation point of view. The same holds for $G(x)$ and $\tilde{C}(x,0)$, $\tilde{R}(x,t)$ and $\tilde{L}_t(x,t)$, $\tilde{G}(x,t)$ and $\tilde{C}_t(x,t)$. Thus, we make the following variable substitutions:

$$r(x) = R(x) + \tilde{L}(x,0), \tag{43}$$

$$g(x) = G(x) + \tilde{C}(x,0), \tag{44}$$

$$\tilde{r}(x,t) = \tilde{R}(x,t) + \tilde{L}_t(x,t), \tag{45}$$

$$\tilde{g}(x,t) = \tilde{G}(x,t) + \tilde{C}_t(x,t). \tag{46}$$

The parameter $r(x)$ represents resistive losses caused by the series resistance and dispersive inductance, and $g(x)$ represents losses caused by the shunt conductance and dispersive capacitance. Likewise, $\tilde{r}(x,t)$ represents the dispersion in the series resistance and inductance, while $\tilde{g}(x,t)$ represents the dispersion in the shunt conductance and capacitance. Finally, defining the transmission line parameters according to equations (43)-(46) we have

$$\begin{aligned}
\partial_x \begin{pmatrix} V(x,t) \\ I(x,t) \end{pmatrix} &= \begin{pmatrix} 0 & -L(x)\,\partial_t \\ -C(x)\,\partial_t & 0 \end{pmatrix} \begin{pmatrix} V(x,t) \\ I(x,t) \end{pmatrix} \\
&\quad + \begin{pmatrix} 0 & -r(x) - \tilde{r}(x,t)\,* \\ -g(x) - \tilde{g}(x,t)\,* & 0 \end{pmatrix} \begin{pmatrix} V(x,t) \\ I(x,t) \end{pmatrix} \\
&= A(x) \begin{pmatrix} V(x,t) \\ I(x,t) \end{pmatrix} + B(x) \begin{pmatrix} V(x,t) \\ I(x,t) \end{pmatrix}.
\end{aligned} \tag{47}$$

The left hand side of equation (47) together with the matrix operator $A(x)$ determine the characteristics of (47), i.e., the wavefront velocity. The matrix operator $B(x)$ contains the dissipative and dispersive terms. Note that $B(x)$ is zero on a uniform, lossless transmission line with nondispersive parameters. Thus, the $B(x)$ term is zero on the connected transmission lines at $x < 0$ and $x > l$. In terms of signal propagation the transmission line is characterized by four nondispersive parameters; $L(x), C(x), r(x)$ and $g(x)$, and two dispersive parameters; $\tilde{r}(x,t)$ and $\tilde{g}(x,t)$. It is important to notice that this means that the dispersion in the inductance and series resistance cannot be distinguished in any measurements. The same holds for the dispersion of the capacitance and shunt conductance.

For our specific problem, with the transmission line model given by equations (20)–(22), the parameters in (47) become

$$L(x) = L_{\mathrm{b}}, \tag{48}$$

$$C(x) = C_\infty(x) = C_1 + \frac{\varepsilon'_\infty(x)\,C_2 C_3}{C_2 + C_3\varepsilon'_\infty(x)}, \tag{49}$$

$$r\left(x\right) = \tilde{r}\left(x,t\right) = 0, \tag{50}$$

$$\begin{aligned} g\left(x\right) &= \frac{C_{\mathrm{s}}\left(x\right) - C_{\infty}\left(x\right)}{\tau_{\mathrm{eff}}\left(x\right)} \\ &= C_2 C_3 \left(\varepsilon_{\mathrm{s}}'\left(x\right) - \varepsilon_{\infty}'\left(x\right)\frac{C_2 + C_3\varepsilon_{\mathrm{s}}'\left(x\right)}{C_2 + C_3\varepsilon_{\infty}'\left(x\right)}\right)\frac{1}{\tau_{\mathrm{d}}\left(C_2 + C_3\varepsilon_{\infty}'\left(x\right)\right)}, \end{aligned} \tag{51}$$

$$\begin{aligned} \tilde{g}\left(x,t\right) &= -\frac{C_{\mathrm{s}}\left(x\right) - C_{\infty}\left(x\right)}{\tau_{\mathrm{eff}}^2\left(x\right)}\mathrm{H}\left(t\right)\exp\left(\frac{-t}{\tau_{\mathrm{eff}}\left(x\right)}\right) \\ &= -\mathrm{H}\left(t\right)\frac{C_2 C_3\left(C_2 + C_3\varepsilon_{\mathrm{s}}'\left(x\right)\right)}{\left(\tau_{\mathrm{d}}\left(C_2 + C_3\varepsilon_{\infty}'\left(x\right)\right)\right)^2} \\ &\quad \cdot\left(\varepsilon_{\mathrm{s}}'(x) - \varepsilon_{\infty}'(x)\frac{C_2 + C_3\varepsilon_{\mathrm{s}}'(x)}{C_2 + C_3\varepsilon_{\infty}'(x)}\right)\exp\left(-\frac{t\left(C_2 + C_3\varepsilon_{\mathrm{s}}'(x)\right)}{\tau_{\mathrm{d}}\left(C_2 + C_3\varepsilon_{\infty}'(x)\right)}\right), \end{aligned} \tag{52}$$

where $\varepsilon_{\mathrm{s}}' = \varepsilon_{\mathrm{sand}} + q\left(x\right)\nu\left(\varepsilon_{\mathrm{s}} - 1\right)$ and $\varepsilon_{\infty}' = \varepsilon_{\mathrm{sand}} + q\left(x\right)\nu\left(\varepsilon_{\infty} - 1\right)$.

With the parameter values given in Subsection 3.3, we see that the momentaneous response capacitance $C\left(x\right)$ varies between 38.4 pF/m and 60.7 pF/m as $q$ goes from 0 to 1. This corresponds to a change of the characteristic impedance, $Z\left(x\right)$, and wavefront velocity, $c\left(x\right)$, from 141.5 Ω to 112.6 Ω and from $1.84 \cdot 10^8$ m/s to $1.46 \cdot 10^8$ m/s, respectively.

The shunt conductance $g\left(x\right)$ is zero if $q\left(x\right) = 0$ and depending on $\tau_{\mathrm{d}}$ being 10 ps, 1 ns, 10 ns or 1 μs, $g\left(x\right)$ is 36,2, 0.362, 0.0362 or $0.36 \cdot 10^{-3}$ S/m when $q\left(x\right) = 1$. When $\tau_{\mathrm{d}}$ approaches zero, $g\left(x\right)$ goes to infinity, and at the same time the dispersion kernel $\tilde{g}\left(x,t\right)$ approaches a delta function with area $= -g\left(x\right)$. In this limit the transmission line can be approximated as nondispersive. The corresponding optical response approximation is

$$C_{\mathrm{opt}}\left(x\right) = C_1 + \frac{\varepsilon_{\mathrm{s}}'\left(x\right)C_2 C_3}{C_2 + C_3\varepsilon_{\mathrm{s}}'\left(x\right)}, \tag{53}$$

$$g_{\mathrm{opt}}\left(x\right) = 0, \tag{54}$$

$$\tilde{g}_{\mathrm{opt}}\left(x,t\right) = 0. \tag{55}$$

### 5.1. Wave Splitting

In this section we transform the dependent variables from voltage and current to the split components, denoted $V^+$ and $V^-$. The split components are uncoupled right and left moving waves on lossless, uniform and nondispersive transmission lines, i.e., the split components equals the incoming and outgoing waves at the boundaries of the nonuniform transmission line, $x = 0^-$ and $x = l^+$.

A wave-splitting uncouples the dependent variables in the principal part of the PDE, i.e., diagonalizes the right hand side of equation (47), [7, 1]. The simplest wave-splitting, fulfilling these criteria, is

$$\begin{pmatrix} V^+(x,t) \\ V^-(x,t) \end{pmatrix} \frac{1}{2} \begin{pmatrix} 1 & Z(x) \\ 1 & -Z(x) \end{pmatrix} \begin{pmatrix} V(x,t) \\ I(x,t) \end{pmatrix} \equiv S(x) \begin{pmatrix} V(x,t) \\ I(x,t) \end{pmatrix}, \tag{56}$$

and the inverse transform is

$$\begin{pmatrix} V(x,t) \\ I(x,t) \end{pmatrix} \begin{pmatrix} 1 & 1 \\ Y(x) & -Y(x) \end{pmatrix} \begin{pmatrix} V^+(x,t) \\ V^-(x,t) \end{pmatrix} \equiv S^{-1}(x) \begin{pmatrix} V^+(x,t) \\ V^-(x,t) \end{pmatrix}, \tag{57}$$

where $Z(x)$ and $Y(x)$ are the time domain characteristic impedance and admittance, respectively:

$$Z(x) = \frac{1}{Y(x)} = \sqrt{\frac{L(x)}{C(x)}}. \tag{58}$$

The PDE for the split components is given by (47) and (56)–(57) as

$$\partial_x \begin{pmatrix} V^+(x,t) \\ V^-(x,t) \end{pmatrix} \left(SAS^{-1} + (\partial_x S)\, S^{-1}\right) \begin{pmatrix} V^+(x,t) \\ V^-(x,t) \end{pmatrix} + SBS^{-1} \begin{pmatrix} V^+(x,t) \\ V^-(x,t) \end{pmatrix}, \tag{59}$$

which yields

$$\begin{aligned} \partial_x \begin{pmatrix} V^+ \\ V^- \end{pmatrix} + \frac{1}{c(x)} \partial_t \begin{pmatrix} V^+ \\ V^- \end{pmatrix} &= \begin{pmatrix} \alpha(x) & \beta(x) \\ \gamma(x) & \theta(x) \end{pmatrix} \begin{pmatrix} V^+ \\ V^- \end{pmatrix} \\ &+ \begin{pmatrix} \tilde{\alpha}(x,t)\, * & \tilde{\beta}(x,t)\, * \\ -\tilde{\beta}(x,t)\, * & -\tilde{\alpha}(x,t)\, * \end{pmatrix} \begin{pmatrix} V^+ \\ V^- \end{pmatrix}, \end{aligned} \tag{60}$$

where

$$c(x) = \frac{1}{\sqrt{L(x)\, C(x)}}, \tag{61}$$

is the wavefront velocity and the nondispersive parameters are given by

$$\alpha(x) = \frac{1}{2} \left(Z_x(x)\, Y(x) - g(x)\, Z(x) - r(x)\, Y(x)\right), \tag{62}$$

$$\beta(x) = \frac{1}{2} \left(-Z_x(x)\, Y(x) - g(x)\, Z(x) + r(x)\, Y(x)\right), \tag{63}$$

$$\gamma(x) = \frac{1}{2} \left(-Z_x(x)\, Y(x) + g(x)\, Z(x) - r(x)\, Y(x)\right), \tag{64}$$

$$\theta(x) = \frac{1}{2} \left(Z_x(x)\, Y(x) + g(x)\, Z(x) + r(x)\, Y(x)\right), \tag{65}$$

where $Z_x(x) = \partial_x Z(x)$. Finally, the dispersive parameters are given by

$$\tilde{\alpha}(x,t) = \frac{1}{2}\left(-\tilde{g}(x,t)\, Z(x) - \tilde{r}(x,t)\, Y(x)\right), \tag{66}$$

$$\tilde{\beta}(x,t) = \frac{1}{2}\left(-\tilde{g}(x,t)\, Z(x) + \tilde{r}(x,t)\, Y(x)\right). \tag{67}$$

Equation (60) is the dynamical equation for the split components $V^{\pm}(x,t)$. If the incident signal is continuous in time, we see from (56) that the split components are continuous where $Z(x)$ is continuous, i.e., everywhere except at the boundaries $x = 0$ and $x = l$.

### 5.2. Green's Functions

The general solution of the scattering problem can be expressed in terms of the fundamental solution, which involve Green's functions. In this section, we derive the partial differential equations (PDEs) and the initial and boundary conditions for the Green's functions. We consider the case where we may have an impedance mismatch at $x = l$ but no mismatch at $x = 0$. This is motivated by the fact that a hard reflection at the far side of the line simplifies a two-parameter reconstruction from reflected data, while a hard reflection at the near end only decreases the quality of the information from the reflections [8, 2]. Furthermore, it is also a minor complication to include a far end impedance mismatch while it is more complicated to include a near end mismatch. We thus include the near end mismatch separately in Subsection 5.3. Note however that we are only considering a one-parameter inverse problem here, which means that we will not utilize the hard reflection from the far end in the present inverse method. The general solution for $V^{\pm}(x,t) \in (0,l)$, in the case where the impedance at $x = 0$ is continuous, is given by [9]

$$V^{+}(x, t + \tau(0,x)) = a^{+}(x)\, V_1^{\mathrm{i}}(t) + G_{\mathrm{cd}}^{+}(x,t) * V_1^{\mathrm{i}}(t), \tag{68}$$

$$V^{-}(x, t + \tau(0,x)) = a^{-}(x)\, V_1^{\mathrm{i}}(t - 2\tau x, l) + G_{\mathrm{cd}}^{-}(x,t) * V_1^{\mathrm{i}}(t), \tag{69}$$

where $V_1^{\mathrm{i}}(t) = V^{+}(0^{+}, t)$ is the incident signal from the left on the nonuniform transmission line, $\tau(x_1, x_2)$ is the wavefront travel time from $x_1$ to $x_2$:

$$\tau(x_1, x_2) = \int_{x_1}^{x_2} \frac{\mathrm{d}x}{c(x)}. \tag{70}$$

$a^{+}(x)$ and $a^{-}(x)$ describe the attenuation of the wavefront traveling to the right and left, respectively. The subscript cd on the Green's functions refers to that the impedance is continuous and discontinuous at the near and far end, respectively.

The dynamical equations for the Green's functions, jump and boundary conditions etc., are derived by substituting (68) and (69) into (60) and noting that terms like $(\cdots)\cdot V_1^{\mathrm{i}}(t)$, $(\cdots)\cdot V_1^{\mathrm{i}}(t-2\tau(x,l))$ and $(\cdots)*V_1^{\mathrm{i}}(t)$ are independent since $V_1^{\mathrm{i}}(t)$ is arbitrary. The PDEs for $G_{\mathrm{cd}}^{\pm}$ are found to be

$$\begin{aligned}\partial_x\begin{pmatrix} G_{\mathrm{cd}}^{+} \\ G_{\mathrm{cd}}^{-}\end{pmatrix}-\frac{2}{c(x)}\partial_t\begin{pmatrix} 0 \\ G_{\mathrm{cd}}^{-}\end{pmatrix} &= \begin{pmatrix} \alpha(x) & \beta(x) \\ \gamma(x) & \theta(x)\end{pmatrix}\begin{pmatrix} G_{\mathrm{cd}}^{+} \\ G_{\mathrm{cd}}^{-}\end{pmatrix} \\ &+\begin{pmatrix} \tilde{\alpha}(x,t) & \tilde{\beta}(x,t) \\ -\tilde{\beta}(x,t) & -\tilde{\alpha}(x,t)\end{pmatrix}*\begin{pmatrix} G_{\mathrm{cd}}^{+} \\ G_{\mathrm{cd}}^{-}\end{pmatrix} \\ &+a^{+}(x)\begin{pmatrix} \tilde{\alpha}(x,t) \\ -\tilde{\beta}(x,t)\end{pmatrix}+a^{-}(x)\begin{pmatrix} \tilde{\beta}(x,t-2\tau(x,l)) \\ -\tilde{\alpha}(x,t-2\tau(x,l))\end{pmatrix}, \end{aligned} \tag{71}$$

where the attenuation factors are given by

$$a^{+}(x)=\exp\left(\int_0^x \alpha(x')\,\mathrm{d}x'\right), \tag{72}$$

$$a^{-}(x)=r_l a^{+}(l)\exp\left(\int_l^x \theta(x')\,\mathrm{d}x'\right), \tag{73}$$

where $r_l$ is the reflection coefficient at $x=l$:

$$r_l=\frac{Z_l-Z(l^-)}{Z_l+Z(l^-)}. \tag{74}$$

Note that the attenuation factor $a^{-}(x)$ includes a factor $r_l a^{+}(l)$, which is the relative amplitude of the reflected wavefront at $x=l$. The boundary value of $a^{+}$ at $x=0$ is 1 since the wavefront has not undergone any attenuation there.

We also obtain the following jump and boundary conditions for the Green's functions:

$$G_{\mathrm{cd}}^{-}(x,0^+)=-\frac{1}{2}c(x)\,a^{+}(x)\,\gamma(x), \tag{75}$$

$$\Delta G_{\mathrm{cd}}^{+}(x,2\tau(x,l))=\frac{1}{2}c(x)\,a^{-}(x)\,\beta(x), \tag{76}$$

$$G_{\mathrm{cd}}^{-}(l^-,t)=r_l G_{\mathrm{cd}}^{+}(l^-,t), \tag{77}$$

$$G_{\mathrm{cd}}^{+}(0^+,t)=0, \tag{78}$$

where $\Delta f(x,t)=f(x,t^+)-f(x,t^-)$. The boundary condition (78) is given directly by equation (68), since $V_1^{\mathrm{i}}(t)=V^{+}(0^+,t)$.

Likewise, equation (77) is derived from (68) and (69) and the fact that $V^-(l^+, t) = 0$ (there is no incident wave from the right), using continuity of the voltage and the current.

Equation (71) together with (75)–(78) can accurately and efficiently be solved numerically with the method of characteristics. The jump condition (76) has to be used in the numerical program since it constitutes a discontinuity in $G_{\rm cd}^+$ along the characteristic line of $G_{\rm cd}^+$. There are also discontinuities in $G_{\rm cd}^+$ across the characteristic line $(x, 2\tau(0,l))$, and in $G_{\rm cd}^-$ along the characteristic line $(x, 2\tau(0,l) + 2\tau(x,l))$. However, since these discontinuities occur along the respective characteristic lines, it is not necessary to treat them separately in the numerical program. But, to achieve better accuracy one should include the analytical solution of these discontinuities. By integrating equation (15) along these characteristic lines, using (72)–(78), we obtain

$$\Delta G_{\rm cd}^+(x, 2\tau(0,l)) = -\frac{1}{2}a^+(x)\, c(0)\, a^-(0)\, \beta(0), \tag{79}$$

$$\Delta G_{\rm cd}^-(x, 2\tau(0,l) + 2\tau(x,l)) = r_l \frac{a^-(x)}{a^-(l)} \left(-\frac{1}{2}a^+(l)\, c(0) a^-(0) \beta(0)\right). \tag{80}$$

### 5.3. The Direct Problem

The direct problem is to compute the transient response of the nonuniform transmission line from an incident delta pulse from the left $(x < 0)$. In the previous subsection, we derived the PDEs and boundary conditions needed to compute the Green's functions in the domain $x \in (0,l), t > 0$. In this subsection, we show how to obtain the transient response of the nonuniform transmission line with impedance mismatches at both ends.

The transient response for the nonuniform transmission line with an impedance mismatch at $x = l$ only, is given by

$$V_1^{\rm r}(t) = b^- V_1^{\rm i}(t - 2\tau) + R_{\rm cd}(t) * V_1^{\rm i}(t), \tag{81}$$

where $\tau = \tau(0,l)$ is the one-way travel time, $V_1^{\rm r}(t) = V^-(0^+, t)$ and $V_1^{\rm i}(t)$ is the incident wave at $x = 0^+$, as shown in Figure 1. The reflection factor $b^-$, and the reflection kernel $R_{\rm cd}(t)$, are given by

$$b^- = a^-(0), \tag{82}$$

$$R_{\rm cd}(t) = G_{\rm cd}^-(0^+, t). \tag{83}$$

This is readily derived from equations (68) and (69). The transient response including the impedance mismatch at $x = 0$ is given by

$$V^{\mathrm{r}}(t) = \sum_{k=0}^{\infty} r_k^+ V^{\mathrm{i}}(t - k \cdot 2\tau) + R_{\mathrm{dd}}(t) * V^{\mathrm{i}}(t), \tag{84}$$

where $r_k^+$ is the reflection coefficients of undistorted directly propagated pulses, which arise because of multiple reflections between the impedance discontinuities at $x = 0$ and $x = l$. $V^{\mathrm{i}}(t) = V^+(0^-, t)$ is the incident wave from the left ($x < 0$), and $V^{\mathrm{r}}(t) = V^-(0^-, t)$ is the reflected wave at $x = 0^-$.

We have the equations to compute the transient response, given by (82)–(83). But, since we are studying the scattering problem described by (84), we need to transform the data in (82)–(83) to the latter case. This can be done by utilizing the relation between $V^{\mathrm{i}}$ and $V^{\mathrm{r}}$, and $V_1^{\mathrm{i}}$ and $V_1^{\mathrm{r}}$, which is

$$\begin{pmatrix} V^{\mathrm{r}}(t) \\ V_1^{\mathrm{i}}(t) \end{pmatrix} \begin{pmatrix} r_0 & 1 - r_0 \\ 1 + r_0 & -r_0 \end{pmatrix} \begin{pmatrix} V^{\mathrm{i}}(t) \\ V_1^{\mathrm{r}}(t) \end{pmatrix}, \tag{85}$$

where $r_0$ is the reflection coefficients at $x = 0$:

$$r_0 = \frac{Z(0^+) - Z_0}{Z(0^+) + Z_0}. \tag{86}$$

From (85) we find that

$$\begin{pmatrix} V_1^{\mathrm{i}}(t) \\ V_1^{\mathrm{r}}(t) \end{pmatrix} = \frac{1}{1 - r_0} \begin{pmatrix} -r_0 & 1 \\ 1 & -r_0 \end{pmatrix} \begin{pmatrix} V^{\mathrm{i}}(t) \\ V^{\mathrm{r}}(t) \end{pmatrix}. \tag{87}$$

The relation from $R_{\mathrm{cd}}(t)$ to $R_{\mathrm{dd}}(t)$ is found from equations (81) and (84) by substituting $(V^{\mathrm{i}}(t), V^{\mathrm{r}}(t))$ for $(V_1^{\mathrm{i}}(t), V_1^{\mathrm{r}}(t))$ ((87) in (81)), and using the fact that $V^{\mathrm{i}}(t)$ is arbitrary. For the reflection data we obtain

$$\begin{aligned} r_0^+ &= r_0, & (88)\\ r_k^+ &= \left(1 - (r_0)^2\right) b^- \left(-r_0 b^-\right)^{k-1}, k \geq 1, & (89)\\ R_{\mathrm{dd}}(t) + r_0 R_{\mathrm{cd}}(t) * R_{\mathrm{dd}}(t) &= \left(1 - (r_0)^2\right) R_{\mathrm{cd}}(t) - r_0 b^- R_{\mathrm{dd}}(t - 2\tau) \\ &\quad - r_0 \sum_{k=1}^{\infty} r_k^+ R_{\mathrm{cd}}(t - k \cdot 2\tau). & (90) \end{aligned}$$

Hence, to compute the impulse response (reflection only) for the transmission line with impedance mismatches at both ends, we begin by computing the Green's functions for the transmission line with impedance mismatch at $x = l$ only. For this we use equations (70) to (80) and the method of characteristics [1]. From this we have the reflection kernel $R_{\text{cd}}(t)$, the reflection factor $b^{-}$ and the round trip delay $2\tau$ (equations (82) and (83)).

Finally, to compute the reflection kernel $R_{\text{dd}}(t)$ we first determine the reflection factors $r_k^{+}$ from equations (88) and (89) and then solve the integral equation (90). All these procedures are well posed operations.

## 6. THE INVERSE PROBLEM IN THE FREQUENCY DOMAIN

In this section, we present the frequency domain approach to the inverse problem of determining the moisture parameter $q(x)$, in the interval $x \in [0, l]$. Define an objective functional as follows:

$$J(q) = \sum_{\omega=\omega_{\min}}^{\omega_{\max}} \left| \hat{r}(0, \omega) - \hat{\boldsymbol{r}}_{\text{m}}(\omega) \right|^2, \tag{91}$$

where $\hat{\boldsymbol{r}}_{\text{m}}(\omega)$ is the *measured* reflection coefficient, at a certain number of frequencies in the interval $[\omega_{\min}, \omega_{\max}]$. $\hat{r}(0, \omega)$ is the calculated reflection coefficient, without taking into account the influences from stray capacitances at the connection points; see Subsection 4.2. To solve the inverse problem iteratively with an optimization approach, we need the gradient of the objective functional (91) with respect to the moisture parameter $q(x)$. To calculate the gradient, we essentially follow the approach described in [3].

At each frequency, a small perturbation $\delta q(x)$ in the moisture profile $q(x)$ results in a small perturbation $\hat{\delta r}(x, \omega)$ in the reflection coefficient $\hat{r}(x, \omega)$. Neglecting higher order terms, the ODE for $\hat{\delta r}$ follows from (34) as

$$\partial_x \hat{\delta r} = 2\left(\hat{a} + \hat{b}\hat{r}\right)\hat{\delta r} + 2\hat{r}\hat{\delta a} + \left(1 + \hat{r}^2\right)\hat{\delta b}, \tag{92}$$

where, from (17), (31) and (32), we have ($\hat{\boldsymbol{L}}$ and $\hat{\boldsymbol{R}}$ do not depend on $q$)

$$\hat{\delta a}(x, \omega) = \hat{\delta b}(x, \omega) = \frac{\mathrm{j}\omega}{2} Z_0 \hat{\delta C}(x, \omega), \tag{93}$$

From (35), it follows that the boundary condition for $\hat{\delta r}$ at $x = l$ is

$$\hat{\delta r}(l, \omega) = 0. \tag{94}$$

The resulting perturbation in the objective functional becomes

$$\delta J\left(q\right)=2\sum_{\omega=\omega_{\mathrm{min}}}^{\omega_{\mathrm{max}}}\left(\hat{r}\left(0,\omega\right)-\hat{\boldsymbol{r}}_{\mathrm{m}}\left(\omega\right)\right)^{\oplus}\hat{\delta r}\left(0,\omega\right), \tag{95}$$

where $\oplus$ denotes the complex conjugate. Introducing a *dual* function $\hat{u}\left(x,\omega\right)$, subject to the following boundary condition at $x=0$:

$$\hat{u}\left(0,\omega\right)=\left(\hat{r}\left(0,\omega\right)-\hat{\boldsymbol{r}}_{\mathrm{m}}\left(\omega\right)\right)^{\oplus}, \tag{96}$$

it follows from (96) and (94) that

$$\begin{aligned}\delta J\left(q\right)&=2\mathrm{Re}\sum_{\omega=\omega_{\mathrm{min}}}^{\omega_{\mathrm{max}}}\hat{u}\left(0,\omega\right)\hat{\delta r}\left(0,\omega\right)\\&=-2\int_{0}^{l}\mathrm{Re}\sum_{\omega=\omega_{\mathrm{min}}}^{\omega_{\mathrm{max}}}\left(\partial_{x}\hat{u}\cdot\hat{\delta r}+\hat{u}\cdot\partial_{x}\hat{\delta r}\right)\mathrm{d}x.\end{aligned} \tag{97}$$

Next, substituting (92) for $\partial_{x}\hat{\delta r}$ in (97) and using (93) we obtain

$$\delta J\left(q\right)=-\int_{0}^{l}\mathrm{Re}\sum_{\omega=\omega_{\mathrm{min}}}^{\omega_{\mathrm{max}}}\left(2\left(\partial_{x}\hat{u}+2\left(\hat{a}+\hat{b}\hat{r}\right)\hat{u}\right)\hat{\delta r}+\mathrm{j}\omega Z_{0}\hat{u}(1+\hat{r})^{2}\,\hat{\delta C}\right)\mathrm{d}x. \tag{98}$$

Now, if (for each frequency) the dual function $\hat{u}\left(x,\omega\right)$ obeys the ODE

$$\partial_{x}\hat{u}\left(x\right)+2\left(\hat{a}\left(x\right)+\hat{b}\left(x\right)\hat{r}\left(x\right)\right)\hat{u}\left(x\right)=0, \tag{99}$$

we have from (99) and (98) that the perturbation in the objective functional becomes

$$\delta J\left(q\right)=-\int_{0}^{l}\mathrm{d}x\mathrm{Re}\sum_{\omega=\omega_{\mathrm{min}}}^{\omega=\omega_{\mathrm{max}}}\mathrm{j}\omega Z_{0}\hat{u}\left(x,\omega\right)\left(1+\hat{r}\left(x,\omega\right)\right)^{2}\hat{\delta C}\left(x,\omega\right). \tag{100}$$

Finally, using that to the first order

$$\hat{\delta C}\left(x,\omega\right)=\frac{\partial\hat{C}}{\partial q}\left(x,\omega\right)\delta q\left(x,\omega\right), \tag{101}$$

and identifying (100) as the inner product

$$\delta J\left(q\right)=\int_{0}^{l}\frac{\partial J}{\partial q}\left(x\right)\cdot\delta q\left(x\right)\mathrm{d}x, \tag{102}$$

the gradient is identified as

$$\frac{\partial J}{\partial q}(x) = -\mathrm{Re} \sum_{\omega=\omega_{\min}}^{\omega=\omega_{\max}} \mathrm{j}\omega Z_0 \hat{u}(x,\omega)\left(1+\hat{r}(x,\omega)\right)^2 \frac{\partial \hat{C}}{\partial q}(x,\omega). \quad (103)$$

where it follows from (12) and (9) that

$$\frac{\partial \hat{C}}{\partial q}(x,\omega) = \frac{C_2^2 C_3}{\left(C_2 + \hat{\varepsilon}_{\mathrm{r}}(x,\omega) C_3\right)^2} \cdot \frac{\partial \hat{\varepsilon}_{\mathrm{r}}}{\partial q}(x,\omega) = \frac{\nu C_2^2 C_3 \hat{\chi}_{\mathrm{water}}(\omega)}{\left(C_2 + \hat{\varepsilon}_{\mathrm{r}}(x,\omega) C_3\right)^2} \quad (104)$$

With the gradient available, the objective functional $J$ is diminished with a standard conjugate gradient method [10]. Note that the dual function $\hat{u}(x,\omega)$, that appears in the expression (103) for the gradient, is determined by integrating the ODE (99) in the $+x$ direction starting from the boundary condition (96).

The reconstruction algorithm was implemented numerically with the Matlab software, on a 180 MHz PowerPC. The time needed for a reconstruction of $q(x)$, starting from the initial guess $q(x) = 0$, was found to be around 15 minutes.

## 7. THE INVERSE PROBLEM IN THE TIME DOMAIN

In this section, we present the time domain approach to the inverse problem of reconstructing the soil moisture profile $q(x)$ from a measurement of the reflected signal $V^{\mathrm{r}}(t)$ due to an incident pulse $V^{\mathrm{i}}(t)$. The proposed method is a mixture of an exact analysis and an optimization approach. The optimization approach is used to compute an approximation of the impulse response of the transmission line. An exact inverse method is then used to reconstruct the moisture profile $q(x)$ from the reflection impulse response. The inverse method is exact in the sense that no mathematical approximations are made, but the numerical implementation involves naturally some approximations.

As mentioned in Section 5, the impedance mismatch at $x = 0$ does not contribute with any useful information to the inverse problem. The impedance mismatch only degrades the quality of the useful signal, which originates from continuous reflections of the incident signal as it propagates along the transmission line from $x = 0$ to $x = l$. When the incident signal has propagated through the transmission line, enough information to reconstruct the moisture parameter can be found in the corresponding reflections. That is, we only need one round trip of reflection data to reconstruct the moisture parameter $q(x), x \in [0, l]$. In cases where there are significant hard reflections at both $x = 0$ and $x = l$, it is advantageous to use as few round trips of data as possible.

This is because the hard reflections may contain more energy than the useful signals (continuously scattered) do. As each hard reflection introduces numerical errors in the algorithm, it is clear that one should use data containing as few hard reflections as possible, i.e. only use one round trip of data. In the frequency domain this would mean using frequency intervals of $\frac{1}{2\tau}$, where $\tau$ is the one round trip propagation time on the transmission line.

The first step in the reconstruction procedure is to deconvolve the reflection data with the incident pulse to obtain the reflection impulse response. However, since the impedance mismatch at $x = 0$ only hides the useful signals, we want to de-embed this mismatch from the reflection data, to obtain the reflection impulse response as if the impedance was continuous at $x = 0$. In Subsection, 7.1 we outline how to deconvolve and de-embed the reflection data by means of optimization. In Subsection 7.2, we then outline the procedure to reconstruct the moisture parameter from the reflection impulse response. The input data to the inverse method is the de-embedded and deconvolved data obtained from the procedure described in Subsection 7.1.

## 7.1. De-Embedding of the Transient Response

In this subsection, we show how to deconvolve and de-embed the reflection data in a single procedure. The inputs are $V^{\mathrm{i}}(t)$ and $V^{\mathrm{r}}(t)$, and the outputs are $R_{\mathrm{cd}}(t)$, $r_0$, $b^-$ and $2\tau$. $R_{\mathrm{cd}}(t)$ is the reflection kernel one would obtain from a reflection measurement on a transmission line with matched impedance at $x = 0$.

We begin by deriving the equation for determining $R_{\mathrm{cd}}(t), b^-, r_0$ and $\tau$ from $V^{\mathrm{i}}(t)$ and $V^{\mathrm{r}}(t)$. Equation (85) yields (see also Figure 1)

$$(1 - r_0) V_1^{\mathrm{i}}(t) = V^{\mathrm{i}}(t) - r_0 V^{\mathrm{r}}(t), \tag{105}$$
$$(1 - r_0) V_1^{\mathrm{r}}(t) = V^{\mathrm{r}}(t) - r_0 V^{\mathrm{i}}(t). \tag{106}$$

By substituting these expressions for $V_1^{\mathrm{i}}$ and $V_1^{\mathrm{r}}$ into (81), we get

$$\begin{aligned} V^{\mathrm{r}}(t) - r_0 V^{\mathrm{i}}(t) = {} & b^- \left(V^{\mathrm{i}}(t - 2\tau) - r_0 V^{\mathrm{r}}(t - 2\tau)\right) \\ & + R_{\mathrm{cd}}(t) * \left(V^{\mathrm{i}}(t) - r_0 V^{\mathrm{r}}(t)\right). \end{aligned} \tag{107}$$

$R_{\mathrm{cd}}(t), b^-, r_0$ and $\tau$ are determined from (107) in three steps. First, $r_0$ is determined by matching the very initial time traces of $V^{\mathrm{r}}$ and $V^{\mathrm{i}}$, which correspond to the hard reflection at $x = 0$. Then $b^-$ and $\tau$ are determined from the first hard reflection that arrives from $x = l$, i.e., by matching the signals in a short time interval after $t = 2\tau$. Finally, $R_{\mathrm{cd}}(t)$ is determined by deconvolving equation (107) with a time domain optimization procedure. We have chosen to use a conjugate gradient method [10] to minimize the following cost function:

$$J^{\mathrm{r}} = \int_0^T \left(R_{\mathrm{cd}}(t) * V_2^{\mathrm{i}}(t) - V_R^{\mathrm{m}}(t)\right)^2 \mathrm{d}t, \tag{108}$$

where $T$ is the time period for which $R_{\mathrm{cd}}(t)$ is to be determined, and where

$$V_2^{\mathrm{i}}(t) = V^{\mathrm{i}}(t) - r_0 V^{\mathrm{r}}(t), \tag{109}$$

$$V_{\mathrm{R}}^{\mathrm{m}}(t) = V^{\mathrm{r}}(t) - r_0 V^{\mathrm{i}}(t) - b^{-}\left(V^{\mathrm{i}}(t-2\tau) - r_0 V^{\mathrm{r}}(t-2\tau)\right). \tag{110}$$

The optimization is easily done by using the exact expression for the gradient of $J^{\mathrm{r}}$ with respect to $R_{\mathrm{cd}}(t)$:

$$J_{R_{\mathrm{cd}}}^{\mathrm{r}}(t') = \frac{\delta J^{\mathrm{r}}}{\delta R_{\mathrm{cd}}} \int_{t'}^{T} \left(R_{\mathrm{cd}}(t) * V_2^{\mathrm{i}}(t) - V_{\mathrm{R}}^{\mathrm{m}}(t)\right) V_2^{\mathrm{i}}(t-t')\,\mathrm{d}t. \tag{111}$$

Thus, the impulse response, consisting of $R_{\mathrm{cd}}(t), b^{-}$ and $\tau$, is obtained by deconvolving equation (107). By deconvolving this equation, the impedance mismatch at $x = 0$ is de-embedded from the transient response in the same step as the impulse response is determined.

## 7.2. Reconstruction Procedure

In this subsection, we outline the time domain inverse method to reconstruct $q(x)$ from the one sided reflection impulse response: $R_{\mathrm{cd}}(t), b^{-}$ and $2\tau$. To determine $q(x)$, we also need the reflection factor $r_0$ and the dispersion model of the flat band cable in moist soil, (48)–(52) (or in the optical approximation case, (48), (50) and (53)–(55)).

The reconstruction is based on equation (75) for the initial value $G_{\mathrm{cd}}^{-}(x, 0^{+})$. If the initial value of $G_{\mathrm{cd}}^{-}$ is known, the spatial derivative of $q(x)$ can be determined by using equations (75), (72), (64), (61), (58), (49) and (51). The relation between $G_{\mathrm{cd}}^{-}(x, 0^{+})$ and $\mathrm{d}q(x)/\mathrm{d}x$ is somewhat complicated expression-wise, but straightforward to compute numerically. Hence, from $G_{\mathrm{cd}}^{-}(x, 0^{+})$, we can solve for $\mathrm{d}q(x)/\mathrm{d}x$, and by integration we have $q(x)$.

The moisture profile $q(x)$ is reconstructed from $x = 0$ to $x = l$ by the following procedure:

1. Deconvolve and de-embed the reflection data $V^{\mathrm{i}}(t)$ and $V^{\mathrm{r}}(t)$ in order to obtain $R_{\mathrm{cd}}(t), b^{-}, 2\tau$ and $r_0$ (cf. Subsection 7.1)

2. Space and time are discretized as $(x,t) = (x_i, j \cdot \mathrm{d}t)$, where $\mathrm{d}t = 2\tau/n$ and $i \in [0,n]$. Space is discretized nonuniformly whereas time is discretized uniformly. This follows from the method of characteristics; cf. Section 5 or ref. [1].
3. $i = 0$ : Set initial values at $x = 0$: $x_i = 0$, $Z_i = Z_0 (1 + r_0) / (1 - r_0)$, $a_i^+ = 1$, $G_{\mathrm{cd}}^- (i,j) = R_{\mathrm{cd}} (j \cdot \mathrm{d}t)$ and $G_{\mathrm{cd}}^+ (i,j) = 0$. Finally, $L_i$, $\mathrm{d}L_i/\mathrm{d}x$ and $r_i$ are given by (48) and (50).
4. $i = 0$ : Compute $q_i$ from $Z_i$ and $L_i$ using (49). Then compute $\mathrm{d}q_i/\mathrm{d}x$ from $G_{\mathrm{cd}}^- (i,0)$ using equations (75), (72), (64), (61), (58), (49) and (51). This determines all the electrical parameters at $x = 0$.
5. $i = i + 1$ : Estimate $x_i$ and the electrical parameters at $x_i$ from the parameter values at $x_{i-1}$.
6. Compute $G_{\mathrm{cd}}^{\pm} (i,0)$ from the electrical parameter values at $x_i$ and $x_{i-1}$, and $G_{\mathrm{cd}}^{\pm} (i-1,[0,1])$.
7. Compute $\mathrm{d}q_i/\mathrm{d}x$ from $G_{\mathrm{cd}}^- (i,0)$ (cf. step 4 above). With the new $\mathrm{d}q_i/\mathrm{d}x$, recalculate $q_i$. Then, based on the new $q_i$, recalculate the electrical parameters, as well as $x_i$.
8. Repeat steps 6 and 7 a few times to improve the accuracy of the reconstructed $q_i$.
9. Compute $G_{\mathrm{cd}}^{\pm} (i,[1,n-1])$
10. If $x_i < l$, go to step 5, else end.

The above procedure involves some interaction in determining $b^-$, $r_0$ and $2\tau$ in the deconvolution/de-embedding procedure. However, it turns out that the reconstruction is insensitive to errors in these parameters. $b^-$ is needed in the de-embedding procedure, but not later in the reconstruction of $q(x)$. Hence, the choice of $b^-$ is not critical. $b^-$ does however influence the accuracy of $q$ close to $x = l$. Likewise, the determination of the round trip delay $2\tau$ is not crucial. This time only sets the limit for how far into the transmission line $q$ can be determined. A somewhat too large value is therefore to prefer over a too small value. $r_0$ is the most important parameter. An accurate determination of $r_0$ improves the reconstruction of $q$ at $x = 0$. Since the reconstruction procedure is sequential and starts at $x = 0$, one expects it to be important to have a small error at $x = 0$. However, it turns out that the method is not very sensitive to errors in $r_0$, but, the larger the error in $r_0$ is, the larger the erroneous region of $q$ at $x = 0$ becomes.

The numerical implementation of the inverse method followed second order approximations. Because of the convolution integrals in the PDEs, the computational load increases as $n^3$ as the number of discretization intervals increases. For $n$ in the order of 1000, the computational time is in the order of 10 seconds for a 180 MHz PowerPC. For a realistic reconstruction that aims at a resolution along the transmission line of 10 to 100 steps, the computational time is less than one second.

## 8. NUMERICAL RESULTS

First we present a comparison between the solutions to the direct problem when using the frequency domain and time domain direct solvers, respectively. Next, we present the reconstructions obtained when using the frequency domain and time domain inverse solvers, respectively, on simulated noisy measurement data generated in the frequency domain. After that we present the reconstructions obtained when using the frequency domain and time domain inverse solvers, respectively, on simulated noisy measurement data generated in the time domain. Finally, we present the reconstructions obtained when using the frequency domain and time domain inverse solvers, respectively, on simulated clean measurement data generated in the frequency domain but with stray capacitances at the endpoints of the band cable. In all numerical examples, we consider four different values of the Debye relaxation time $\tau_{\rm d}$: 10 ps, 1 ns, 10 ns and 1 $\mu$s.

### 8.1. Comparisons of the Solutions Obtained to the Direct Problem Using Frequency and Time domain Direct Solvers, Respectively

In the time domain, the reflection kernels were computed as described in Section 5. For the shortest relaxation time of 10 ps, the computation became very slow since the resolution of the dispersion kernel then required a very fine discretization in the time variable. To circumvent this problem, the optical response approximation, described by (53)–(55), was used in the time domain instead of the dispersion model (20), when $\tau_{\rm d} = 10$ ps. The reflected voltages due to an incident voltage in the form of a gaussian pulse with a peak value of 1 V and a half width of 1 ns were then obtained through convolution with the reflection kernels. In the frequency domain, the corresponding reflection coefficients were calculated, as described in Subsection 4.1, for frequencies from 0 Hz in step of 10 MHz up to 3 GHz, where the spectrum of the gaussian pulse is diminished effectively. The reflected voltages, obtained by multiplying the reflection coefficients with the spectrum of the gaussian pulse, were then transformed to the time domain by means of an inverse fast fourier transform (IFFT) in which we used a sampling frequency of 60 GHz. The reflected voltages at $x = 0^-$ are depicted in Figure 4, where we in Figures 4(b), 4(c) and 4(d) see an excellent agreement between the results obtained for $\tau_\mathrm{d} = 1\,\mathrm{ns}$, $\tau_\mathrm{d} = 10\,\mathrm{ns}$ and $\tau_\mathrm{d} = 1\,\mu\mathrm{s}$, respectively (the incident pulse has its peak value at $x = 0^-$ when $t = 3\,\mathrm{ns}$). In Figure 4(a) ($\tau_\mathrm{d} = 10\,\mathrm{ps}$) we see small discrepancies for the later times. This is because an optic response approximation was used in the time domain.

## 8.2. Reconstructions Using Noise Contaminated Data Generated in the Frequency Domain

The frequency domain direct solver was used to generate clean reflection data in the interval 0 Hz to 1 GHz with 10 MHz spacing between the frequencies. To simulate noise contaminated measurement data, gaussian noise with a zero mean value and a standard deviation of 0.025 was added on both the real and the imaginary part of the calculated reflection coefficient.

To avoid problems with local minima in the objective functional (91), when using the frequency domain method, the initial minimization must be carried out using frequencies up to around 100 MHz only which yields a rough initial reconstruction. Then one successively incorporates higher frequencies to obtain a more detailed reconstruction. The reconstructions obtained for the moisture parameter $q\,(x)$ when using the FD method are shown in Figure 5, where we notice good agreements with the true profile except for the case when $\tau_\mathrm{d} = 1\,\mathrm{ns}$. A probable explanation for this is that we have very high losses in the region where $q\,(x) \neq 0$ when $\tau_\mathrm{d} = 1\,\mathrm{ns}$. Waves with higher frequencies will then suffer a strong attenuation and can consequently not reach into the far end region of the transmission line; cf. the longer period in the oscillations in the reconstructed profile in the region $x > 0.4\,\mathrm{m}$.

The frequency domain data were then transformed to the time domain by means of IFFT. To obtain a more localized incident pulse in the time domain, the FD data was multiplied with the following Kaisser-Bessel filter function, before the IFFT:

$$H\,(f) = \frac{\sin\left(\sqrt{\left(\frac{\pi f}{f_0}\right)^2 - \beta^2}\right)}{\mathrm{I}_0\,(\beta)\sqrt{\frac{\pi f}{f_0}^2 - \beta^2}}, \tag{112}$$

where we used $f_0 = 1\,\mathrm{GHz}$ and $\beta = 0.1$.

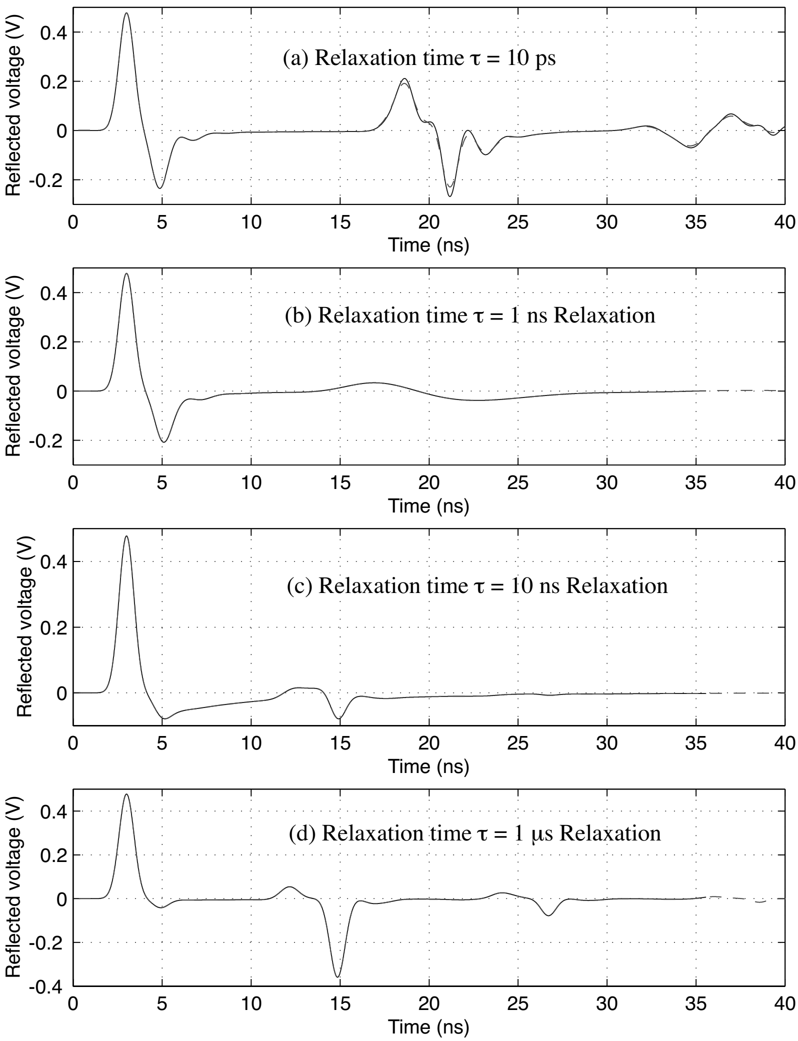


**Figure 4.** The reflected voltage as a function of time, for different values of the relaxation time $\tau_\mathrm{d}$ in the Debye model. The incident voltage is a gaussian pulse with a peak value of 1 V and half width of 1 ns. The solid lines depict the results obtained by using the time domain method and the dashed lines depict the results obtained from an inverse discrete fourier transform of the data generated with the frequency domain method.

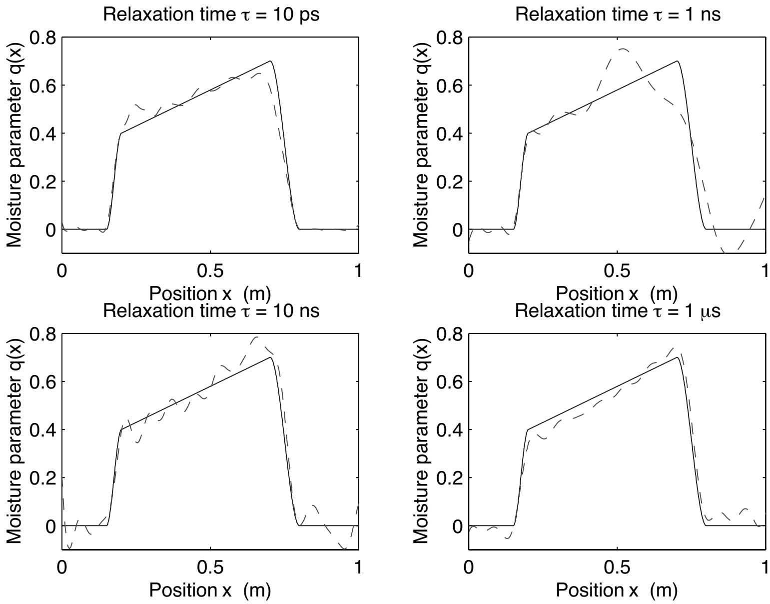


**Figure 5.** Frequency domain reconstruction of the moisture parameter $q\,(x)$ using artificial noisy data generated in the frequency domain; the true profile is given by solid lines and the reconstructed profiles are given by dashed lines.

First, the transient response of the band cable was de-embedded from the TD data, as described in Subsection 7.1. The results of the de-embedding are shown in Table 1. After that, the moisture profile $q\,(x)$ was reconstructed using the TD inversion algorithm. The reconstructions obtained are shown in Figure 6. In conformance with the results from using the FD method, we see in Figure 6 good agreements with the true profile except for the case when $\tau_{\mathrm{d}} = 1\,\mathrm{ns}$, where the TD inverse code fails at $x = 0.4\,\mathrm{m}$ because the directly propagating signal becomes too weak in that region. The TD inverse algorithm explicitly uses the amplitude of the directly propagating signal. Hence, if that is too small the algorithm becomes sensitive to numerical and measurement errors. The amplitude of the hard reflection from $x = l$ indicates the amplitude of the received useful signal from the far end of the line. In Table 2, we see that the first hard reflection, $r_1^+$, from the far end of the line is negligibly small for $\tau_{\mathrm{d}} = 1\,\mathrm{ns}$. For $\tau_{\mathrm{d}} = 10\,\mathrm{ps}$ the exact $r_1^+$ is actually even smaller and a reconstruction would therefore seem to be impossible. However, since we aim for a reconstruction resolution of about $5\,\mathrm{cm}$, we only

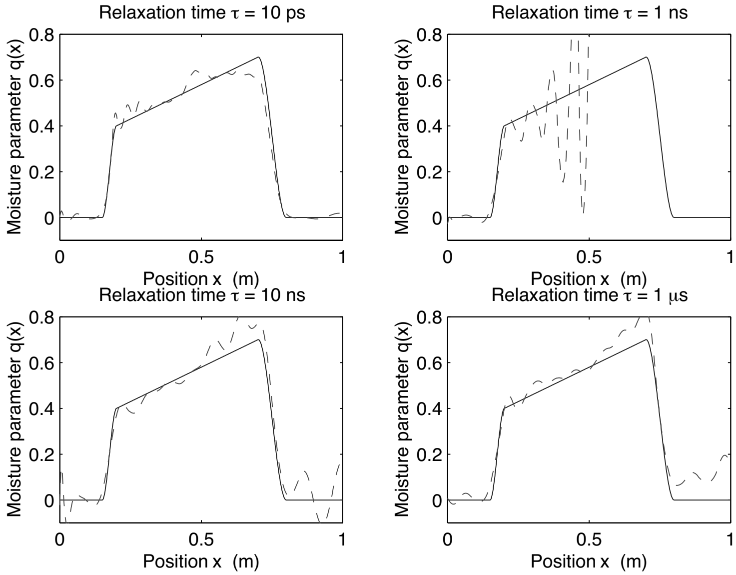


**Figure 6.** Time domain reconstruction of the moisture parameter $q(x)$ using IFFT transformed artificial noisy data generated in the frequency domain; the true profile is given by solid lines and the reconstructed profiles are given by dashed lines.

**Table 1.** Values used in the deconvolution and de-embedding.

| Debye relaxation time $\tau_{\mathrm{d}}$ | 10 ps | 1 ns | 10 ns | 1 $\mu$s |
|---|---|---|---|---|
| Estimated $r_0$ | 0.473 | 0.481 | 0.481 | 0.477 |
| Estimated $b^-$ | -0.3 | 0 | -0.106 | -0.47 |
| Estimated roundtrip time $2\tau$ | 18.1 ns | 25.0 ns | 11.9 ns | 11.9 ns |
| Time intervals in reconstructed $R_{\mathrm{cd}}$ | 250 | 250 | 250 | 33 |
| Time intervals used in deconvolution | 500 | 500 | 500 | 500 |

need an incident pulse width of around 1 ns. The pulse width is hence long as compared with the relaxation time of 10 ps, and the optical response approximation can therefore be assumed valid. This assumption is verified by the good agreement in the direct problem as shown in Figure 4. Using the optical response approximation, we get the reflection factor $r_1^+$ as shown in Table 2.

In Figure 4, one can clearly see that the reflected signal for the

**Table 2.** Reflection factors obtained in the TD direct problem for different relaxation times.

| $\tau_{\mathrm{d}}$ | $r_0^+$ | $r_1^+$ | $r_2^+$ | $b^-$ |
|---|---|---|---|---|
| 10 ps | 0.478 | -0.369 | -0.0842 | -0.478 |
| 1 ns | 0.478 | $-8.89 \cdot 10^{-8}$ | $-4.89 \cdot 10^{-15}$ | $-1.15 \cdot 10^{-7}$ |
| 10 ns | 0.478 | -0.0834 | -0.00400 | -0.104 |
| 1 $\mu$s | 0.478 | -0.363 | -0.0817 | -0.471 |

case with $\tau_{\mathrm{d}} = 1\,\mathrm{ns}$ contains no visible hard reflection from $x = l$, whereas such reflections are seen for the other relaxation times. What is interesting to notice is that the reconstruction problem in the 1 ns case is also seen in the FD method, which do not explicitly use the directly propagating signals. It can thus be concluded that a parameter reconstruction is based on having a directly propagating signal that resolves the spatial variation via reflections.

### 8.3. Reconstructions Using Noise Contaminated Data Generated in the Time Domain

The time domain direct solver was used to generate clean reflection data. To simulate noise contaminated measurement data, gaussian noise with a zero mean value and a standard deviation of $0.005 \cdot \max\{V^{\mathrm{i}}\}$ was added on both $V^{\mathrm{i}}$ and $V^{\mathrm{r}}$.

The results after de-embedding the transient response from the TD data are shown in Table 3. After that, the moisture profile $q(x)$ was reconstructed using the TD inversion algorithm. The reconstructions obtained are shown in Figure 7, where we see good agreements with the true profile except for the case when $\tau_{\mathrm{d}} = 1\,\mathrm{ns}$, in which the TD algorithm was interrupted by numerical errors (cf. the results in Figure 6 from the previous subsection). The overall quality of the reconstructions obtained using the TD algorithm on TD generated data is slightly better than what was obtained when using the TD algorithm on IFFT transformed FD data.

The noise contaminated TD data were transformed to the frequency domain by means of FFT (with no filtering in advance). The reconstructions obtained when using the frequency domain method are shown in Figure 8. In conformance with the results from using the TD method, we see in Figure 8 good agreements with the true profile except for the case when $\tau_{\mathrm{d}} = 1\,\mathrm{ns}$, where the FD algorithm cannot

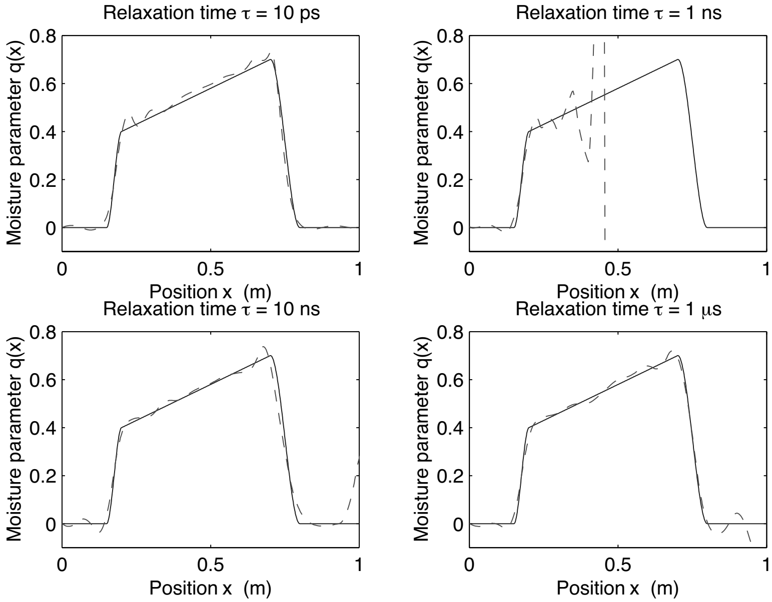


**Figure 7.** Time domain reconstruction of the moisture parameter $q\,(x)$ using artificial noisy data generated in the time domain; the true profile is given by solid lines and the reconstructed profiles are given by dashed lines.

**Table 3.** Values used in the deconvolution and de-embedding.

| Debye relaxation time $\tau_\mathrm{d}$ | 10 ps | 1 ns | 10 ns | 1 $\mu$s |
|---|---|---|---|---|
| Estimated $r_0$ | 0.477 | 0.477 | 0.478 | 0.478 |
| Estimated $b^-$ | -0.45 | 0 | -0.1 | -0.47 |
| Estimated roundtrip time $2\tau$ | 18.2 ns | 19.6 ns | 11.9 ns | 11.8 ns |
| Time intervals in reconstructed $R_\mathrm{cd}$ | 25 | 35 | 25 | 25 |
| Time intervals used in deconvolution | 500 | 500 | 500 | 500 |

reproduce the sharp slope in the profile around $x = 0.75\,\mathrm{m}$ (cf. the results in Figure 5 from the previous subsection). The reconstructions obtained using the FD algorithm on TD generated data that has been transformed with FFT exhibit slightly more oscillations superimposed on the true profile, but are otherwise of the same quality as the ones obtained when using the FD algorithm on FD generated data.

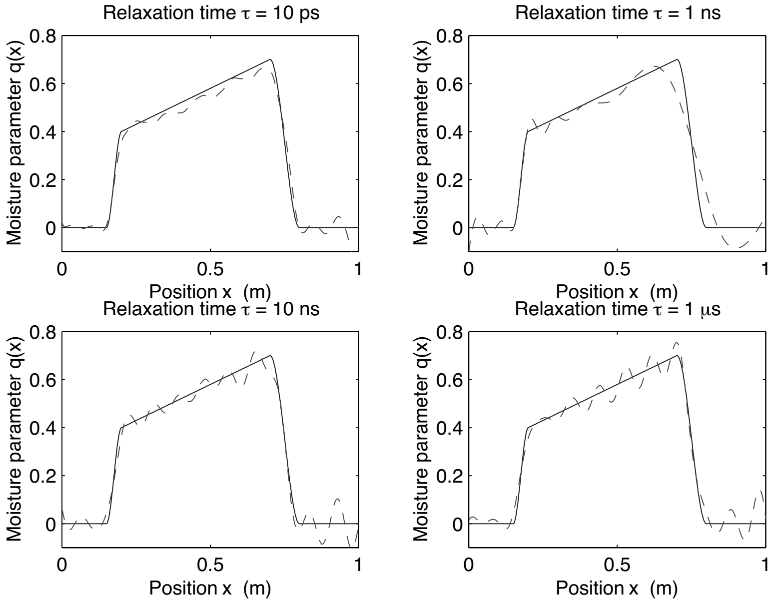


**Figure 8.** Frequency domain reconstruction of the moisture parameter $q\,(x)$ using FFT transformed artificial noisy data generated in the time domain; the true profile is given by solid lines and the reconstructed profiles are given by dashed lines.

## 8.4. Reconstructions Using Frequency Domain Data Generated with Stray Capacitances at the Endpoints of the Band Cable

The frequency domain direct solver was modified, as described in Subsection 4.2, to generate clean reflection data influenced by two stray capacitances $C_0 = C_l = 2\,\mathrm{pF}$ connected at the endpoints of the band cable; data were then generated from 0 Hz to 1 GHz with 10 MHz spacing. The reconstructions obtained for the moisture parameter $q\,(x)$ when using the frequency domain method are shown in Figure 9. The result for $\tau_\mathrm{d} = 10\,\mathrm{ps}$ shows good agreement, but the influence of the stray capacitance $C_0$ at $x = 0\,\mathrm{m}$ can be seen clearly, since $q(x = 0)$ becomes rather high. The results when using the longer relaxation times are heavily distorted by oscillations superimposed on the true profile and the influence of $C_0$ at $x = 0\,\mathrm{m}$ can be seen clearly, since $q(x = 0) \geq 1$ (which is unphysical with the model used). For all relaxation times considered, there is no noticeable influence of the capacitance $C_l$ at $x = 1\,\mathrm{m}$, in terms of an increased value of $q(x = 1)$.

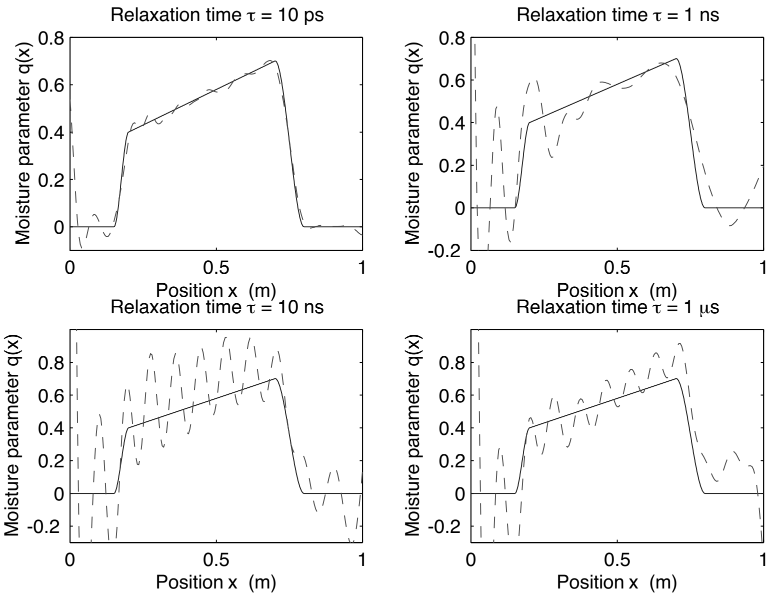


**Figure 9.** Frequency domain reconstruction of the moisture parameter $q(x)$ using artificial clean data generated in the frequency domain but with stray capacitances at the endpoints of the band cable; the true profile is given by solid lines and the reconstructed profiles are given by dashed lines.

The TD data was obtained by IFFT after the FD data had been multiplied with the filter function (112). The results after de-embedding the transient response are shown in Table 4. The reconstructions obtained after using the TD algorithm on the transient responses are shown in Figure 10. The result for $\tau_\mathrm{d} = 10\,\mathrm{ps}$ shows good agreement, with no visible influences from the stray capacitances in terms of increasing values of $q$ near the endpoints. For $\tau_\mathrm{d} = 1\,\mathrm{ns}$ the TD algorithm once again fails due to numerical imbalance. For the relaxation times, $\tau_\mathrm{d} = 10\,\mathrm{ns}$ and $\tau_\mathrm{d} = 1\,\mu\mathrm{s}$, there are no increases of $q$ near the endpoints and no oscillations, which were the cases when using the FD algorithm, but the reconstructed profiles become shifted downwards in comparison with the true profile, especially when $\tau_\mathrm{d} = 1\,\mu\mathrm{s}$.

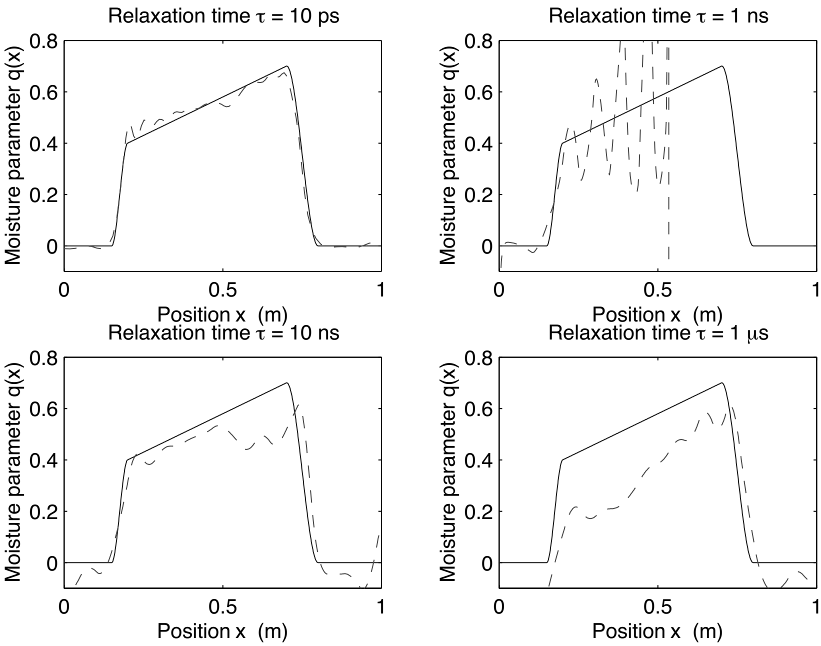


**Figure 10.** Time domain reconstruction of the moisture parameter $q(x)$ using IFFT transformed artificial clean data generated in the frequency domain but with stray capacitances at the endpoints of the band cable; the true profile is given by solid lines and the reconstructed profiles are given by dashed lines.

**Table 4.** Values used in the deconvolution and de-embedding.

| Debye relaxation time $\tau_d$ | 10 ps | 1 ns | 10 ns | 1 $\mu$s |
|---|---|---|---|---|
| Estimated $r_0$ | 0.505 | 0.515 | 0.515 | 0.505 |
| Estimated $b^-$ | -0.35 | 0 | -0.11 | -0.49 |
| Estimated roundtrip time $2\tau$ | 18.0 ns | 18.0 ns | 11.8 ns | 11.7 ns |
| Time intervals in reconstructed $R_{cd}$ | 40 | 30 | 40 | 40 |
| Time intervals used in deconvolution | 500 | 500 | 500 | 500 |

## 9. DISCUSSION AND CONCLUSIONS

In this paper, we have compared the FD and TD direct and inverse algorithms for a nonuniform and dispersive transmission line, for the special case of reconstructing the relative water content in moist sand. The influence of stray capacitances at the end points has been investigated also.

Regarding that the TD algorithm was implemented numerically with compiled C-code whilst the FD algorithm was implemented with slower interpreting Matlab code, our conclusion is anyway that the TD algorithm is computationally faster than the FD algorithm. On the other hand, at present we have not automated the determination of $R_{\mathrm{cd}}$, $r_0$, $b^-$ and $2\tau$. These parameters are thus determined interactively with the help of a program. In difficult cases, this process may require some skills. However, $b^-$ is not very important at all and the TD method is robust to errors in both $r_0$ and $2\tau$.

The conclusion from the comparisons of the direct solvers is that both direct solvers work fine, and that there is no difference in generating the data in either domain. Hence, there is no reason to by default use an inverse analysis in the same domain as the measurement is performed in as long as the band width in the frequency domain allows a transformation to the time domain and vice versa.

When reconstructing from FD generated data, a general impression is that the FD and TD inverse methods are equally accurate. It was interesting to notice that both method failed at $x = 0.4\,\mathrm{m}$ in the case when $\tau_{\mathrm{d}} = 1\,\mathrm{ns}$. Since the TD method is based on an exact algorithm, the reconstruction fails completely at $x > 0.4\,\mathrm{m}$. In the FD method, which is based on optimization, the algorithm is robust against high values of the loss parameters, but the high frequency components of the gradient then become attenuated which prevents from reconstructing rapidly varying parameters. When reconstructing from TD generated data, the reconstructions obtained using the TD method exhibit less ripple than the ones obtained from the FD method, which might be a consequence of that the TD method uses one round trip of data only and thus suppresses errors due to multiple reflections between $x = 0$ and $x = l$. When the artificial measurement data were generated with stray capacitances at the end points of the band cable, we obtained significant errors in the reconstructed profiles when using both the FD and TD inversion algorithms, respectively. Thus, it is of crucial importance that the stray capacitances can be estimated accurately, in order to be incorporated into the FD and TD inversion algorithms, respectively.

## REFERENCES

1. Lundstedt, J. and S. Ström, "Simultaneous reconstruction of two parameters from the transient response of a nonuniform LCRG transmission line," *J. Electro. Waves and Applic.*, Vol. 10, 19–50, 1996.
2. Lundstedt, J. and S. He, "A time domain optimization technique for the simultaneous reconstruction of the characteristic impedance, resistance and conductance of a transmission line," *J. Electro. Waves and Applic.*, Vol. 10, 581–601, 1996.
3. Norgren, M. and S. He, "An optimization approach to the frequency-domain inverse problem for a nonuniform LCRG transmission line," *IEEE Transactions on Microwave Theory and Techniques*, Vol. 44, 1503–1507, 1996.
4. Norgren, M. and S. He, "Optimal designs for nonuniform LCRG transmission lines," *J. Electro. Waves and Applic.*, Vol. 10, 1113–1127, 1996.
5. Kristensson, G., S. Rikte, and A. Sihvola, "Mixing formulas in the time domain," *J. Opt. Soc. Am. A*, Vol. 15, 1411–1422, 1998.
6. Scaife, B. K. P., *Principles of Dielectrics*, Clarendon Press, Oxford, 1989.
7. Hellberg, R. and A. Karlsson, "Design of reflectionless media for transient electromagnetic waves," *Inverse Problems*, Vol. 11, 147–164, 1995.
8. Kristensson, G. and R. J. Krueger, "Direct and inverse scattering in the time domain for a dissipative wave equation. Part 4: Use of phase velocity mismatches to simplify inversions," *Inverse Problems*, Vol. 5, 375–388, 1989.
9. Fuks, P., A. Karlsson, and G. Larson, "Direct and inverse scattering from dispersive media," *Inverse Problems*, Vol. 10, 555–571, 1994.
10. Polak, E., *Computational Methods in Optimization*, Academic Press, 77 New York and London, 1971.